Enhanced momentum delivery by electric force to ions due to collisions of ions with neutrals

G. Makrinich and A. Fruchtman

Citation: Phys. Plasmas **20**, 043509 (2013); doi: 10.1063/1.4800012
View online: http://dx.doi.org/10.1063/1.4800012
View Table of Contents: http://pop.aip.org/resource/1/PHPAEN/v20/i4
Published by the American Institute of Physics.

Enhanced momentum delivery by electric force to ions due to collisions of ions with neutrals

G. Makrinich and A. Fruchtman
H.I.T.—Holon Institute of Technology, Holon 5810201, Israel

(Received 21 January 2013; accepted 22 March 2013; published online 10 April 2013)

Ions in partially ionized argon, nitrogen, and helium gas discharges are accelerated across a magnetic field by an applied electric field, colliding with neutrals during the acceleration. The momentum delivered by the electric force to the ions, which is equal to the momentum carried by the mixed ion-neutral flow, is found by measuring the force exerted on a balance force meter by that flow exiting the discharge. The power deposited in the ions is calculated by measuring the ion flux and the accelerating voltage. The ratio of force over power is found for the three gases, while the gas flow rates and magnetic field intensities are varied over a wide range of values, resulting in a wide range of gas pressures and applied voltages. The measurements for the three different gases confirm our previous suggestion [G. Makrinich and A. Fruchtman, Appl. Phys. Lett. **95**, 181504 (2009)] that the momentum delivered to the ions for a given power is enhanced by ion-neutral collisions during the acceleration and that this enhancement is proportional to the square root of the number of ion-neutral collisions. © *2013 American Institute of Physics*. [http://dx.doi.org/10.1063/1.4800012]

I. INTRODUCTION

The momentum carried by a flowing gas is an important characteristic because of its effect on the interaction with surfaces[1–4] and for electric propulsion.[5–7] Often the gas acquires momentum through a full or partial ionization and a subsequent acceleration of the charged particles across an applied voltage. When the ionization is only partial, the momentum acquired by the charged ions can be redistributed between all particles through collisions between ions and neutrals. This redistribution of momentum that results in energetic neutrals might be advantageous for certain industrial processes. We have shown recently that if the ion-neutral collisions occur during the acceleration of the ions by the electric field, the total momentum gained by the ion flow (and distributed between both ions and neutrals) is enhanced considerably.[8–10] Enhancement of the momentum delivered by the electric field through ion-neutral collision is used in ionic wind propulsion employing high-voltage corona discharges.[11–14] The thrust is provided by the electric pressure and is limited by space charge of the ion flow.[15] In our configuration, the ions are accelerated in quasi-neutral plasma, where electrons are magnetized, and the thrust is provided by magnetic pressure.

Our purpose in the current study is to investigate the rate of enhancement of the momentum delivery by ion-neutral collisions. Our previous studies[8,9] were done in argon discharge only and for a limited range of pressure and magnetic field intensity. Here, we extend our measurements to three gases, argon, nitrogen, and helium, and for a large range of pressures and magnetic field intensities. We are then able to show that the momentum enhancement agrees with the theoretical analysis.[8,9]

In Sec. II, we present our previous calculation[8,9] of the enhancement of the momentum due to ion-neutral collisions. We also present an expression for the ratio of the force exerted by the flow over the deposited power. In Sec. III, we describe the experimental setup. The experiments were conducted in our Radial Plasma Source (RPS) which is an upgraded version of our RPS used in previous studies.[8,9] We also describe, first time in detail, our Balance Force Meter (BFM) which we used already in our previous study.[9] The BFM is used for measuring the force exerted by the mixed ion-neutral flow, which equals the rate of momentum delivery to the flow by the electric force. We also describe how we measure the ion current and the accelerating voltage. In Sec. IV, we present the actual measurements of the electric force on the flow, the ion current, and the accelerating voltage. Finally, in Sec. V, we analyze the measurements done for a wide range of parameters for three different gases and show that indeed the momentum is enhanced according to the model presented in Sec. II.

II. FORCE AND POWER

As we have shown,[8,9] the total electric force at each instant on ions that flow across an accelerating voltage, while they are colliding with neutrals, is

$$F_E = m\Gamma_i v_0 \sqrt{\frac{a}{2\lambda}}. \tag{1}$$

Here, m is the ion mass, Γ_i is the ion particle flux, a is the length of the acceleration region, and λ is the ion-neutral collision mean-free-path. The maximal ion velocity is $v_0 \equiv \sqrt{2eV_{ac}/m}$, V_{ac} being the accelerating voltage and e is the elementary charge. This force equals the momentum per unit time carried by the mixed ion-neutral flow that exits the acceleration region, a momentum that was delivered to the ions by the electric force and was redistributed between the ions and the neutrals through collisions. In deriving Eq. (1), we assumed that the electric field and λ are constant along

the ion acceleration and that the ion-neutral collision frequency is v_i/λ, v_i being the ion fluid velocity. We further assumed that there is no ionization in the acceleration region so that the ion particle flux is constant. Equation (1) is an approximation of the force for the regime of a large number of ion-neutral collisions so that

$$\lambda \ll a. \tag{2}$$

Equation (1) expresses the increase of the electric force exerted on the ions by ion-neutral collisions, relative to the case that ions are collisionless. The force is enhanced by $\sqrt{a/2\lambda}$. Equation (1) also describes the equivalent enhancement by $\sqrt{a/2\lambda}$ of the momentum delivered by the electric force to the ions, and, through collisions, to the ion-neutral flow. At the limit $\lambda \ll a$ the ions transfer through collisions most of the momentum that they gain from the electric force to the neutral gas.

We emphasize that the process in which we are interested is not only the transfer of momentum that ions gain by electric force to neutral gas. For such a process to occur, it is enough that the ions collide with a neutral gas after they have been accelerated. If the ion acceleration and the momentum-transfer collisions occur in the same region simultaneously, however, momentum is not only transferred to the neutral-gas but also the total momentum delivered by the electric force to the ion-neutral flow is greatly increased.

Our purpose is to examine whether the enhancement of momentum delivery to the flow actually happens and whether the momentum delivery indeed obeys the scaling described by Eq. (1). We measure the momentum carried by the flow by measuring the force exerted by the flow on the surface of our BFM. If the flow that exits the acceleration region impinges on a surface and loses all its momentum (but without being reflected), then the force exerted on the surface equals the rate of the momentum loss, which, in turn, equals the electric force that was exerted on the ions. We can then test whether that measured force agrees with the force calculated according to Eq. (1).

One important application of the present study is electric propulsion. An important figure of merit for propulsion is the ratio of thrust over power. The thrust on a spacecraft equals the force exerted on the propellant that exits the thruster. The power deposited in the ions for acceleration is

$$P_i = e\Gamma_i V_{ac}. \tag{3}$$

We assume again that all the ions move across the full accelerating voltage. Obviously, the power deposited in the plasma is larger and includes the power deposited in the electrons. We calculate here the ratio of the force over the power deposited in the ions, employing Eqs. (1) and (3). The ratio is thus written as

$$\frac{F_E}{P_i} = \frac{2}{v_0}\sqrt{\frac{a}{2\lambda}}. \tag{4}$$

The ratio of force over power is also enhanced by $\sqrt{a/2\lambda}$ relative to the case that ions do not collide.

For the comparison of the theoretical expression to experimental measurements, we substitute into Eq. (4) $\lambda = 1/\sigma N, \sigma$ is the ion-neutral collision cross-section and N is the neutral gas density. Equation (4) takes therefore the form

$$\frac{F_E}{P_i} = \sqrt{\frac{m\sigma N a}{V_{ac}}}. \tag{5}$$

In the next sections, we describe how we measure F_E, P_i, and V_{ac} in order to test whether Eq. (5) is satisfied. In Sec. III, we describe the experimental setup, the plasma source and the measurements methods.

III. EXPERIMENTAL SETUP

In this section, we describe our plasma source (subsection III A), the measurement of the electric force (subsection III B), and the ion current and accelerating voltage (subsection III C).

A. Plasma source

The RPS[8,9] has been upgraded by introducing a new magnetic circuit that allows generating a larger magnetic field and a new gas distributor that distributes the gas more uniformly. The upgraded RPS shown in Fig. 1 consists of a ceramic insulator, a molybdenum anode, a magnetic-field generating solenoid, an iron core, a (new) gas distributor and a cathode. The ceramic insulator is composed of two annular disks and an axial segment glued together. The outer diameter of each of the annular disks is 86 mm, the inner diameter 30 mm, and the axial distance between the two disks 8.5 mm. The anode is a molybdenum wire of 2 mm diameter that has a ring shape of 50 mm diameter. Together with the iron core, the solenoid generates an axial magnetic field that is concentrated at the outer edge of the iron core. For a dc current of 4 A, the maximal magnetic field at the edge is 420 G (relative to maximum 180 G in the previous version[8,9]). The working gas is injected into the space between the two disks of ceramic insulator through the gas distributor. The gas distributor consists of a central channel along the RPS axis, through which the gas flows into six elongated holes (two of the holes are seen in Fig. 1) of 24 mm length and 2 mm diameter. The central part of the gas distributor is embedded in the iron core. As described below, three different gases were used in

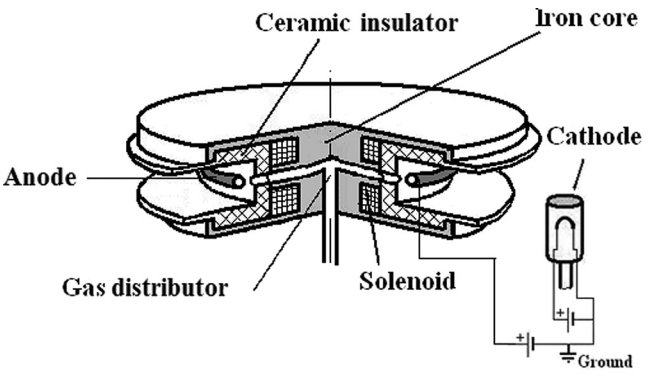

FIG. 1. The Radial Plasma Source.

the experiment with various gas flow rates [argon 30–320 SCCM (Standard Cubic Centimeters per Minute), nitrogen 75–350 SCCM and helium 415–600 SCCM], and consequently, the pressure in the vacuum chamber varied (argon 4.3–68 mTorr, nitrogen 9.3-82 mTorr, and helium 150-300 mTorr). The pressure was measured at a distance of 50 cm from the RPS center by two pressure manometers: the Baratron 627 for pressures up to 0.05 Torr with a precision 0.15% and the Baratron 626 for pressures up to 2 Torr with a precision 0.25%.

A cathode is located at a distance of 8 cm from the RPS axis. A voltage that is applied between the anode and the cathode ignites a discharge and accelerates the plasma ions radially outward across the axial magnetic field. Because of the axial magnetic field, the electrons are expected to drift azimuthally around the RPS and to move radially inward due to collisions towards the anode. Indeed, when the magnetic field is applied the discharge seems to be azimuthally uniform.[8] The cathode also serves as a neutralizer of the ion-flow current, by providing electrons that follow the ions that leave the RPS in the radial direction. The cathode emits electrons by heating a five-turn tungsten loop filament of 10 mm diameter and 15 mm height, by a dc current of 19 A. The loop is positioned inside a molybdenum cylinder in order to reduce heating other parts of the source. A working gas of 4 SCCM gas flow rate flows through the cathode.[8]

The RPS is positioned at the center of a cross ISO-320 vacuum chamber.[8] The vacuum chamber is equipped with pressure measurement gauges and three gas flow meters and is pumped to a base pressure of 0.01 mTorr by mechanical and turbomolecular pumps. The procedure of the discharge ignition and the RPS operation was described previously also in Ref. 8.

In the experiments described here, the discharge current was a chosen to be 1.1 A. For this value of the discharge current, the RPS discharge was stable for a large range of values of magnetic field and gas flow rate of the three used gases.

B. Balance force meter

As explained in Sec. II, we evaluate the electric force on the ions, which equals the momentum flux carried by the flow, by measuring the force exerted by that flow while impinging on a sensing surface of our BFM. The force exerted by the flow is the net force measured by the BFM, which is the difference between the two forces acting in opposite directions on the upstream and downstream sides.[8] Similarly to other impact force meters,[16–21] the BFM measures the force by balancing its torque with the torque of a calibrated other force. In our first study,[8] the calibrated force used in our BFM was gravity, as the sensitive plate was a part of a pendulum. In our later study,[9] the BFM has been modified, and a calibrated magnetic force was used as a balancing force. Here, we describe in more detail the modified BFM, which we also used in the present study.

The BFM is shown in Fig. 2. A force was exerted by the flow on a sensing plate (20.2×20.2 mm^2), made of mica, that is a part of a pendulum. The motion of the sensing plate caused a motion of the attached aluminum reflecting plate,

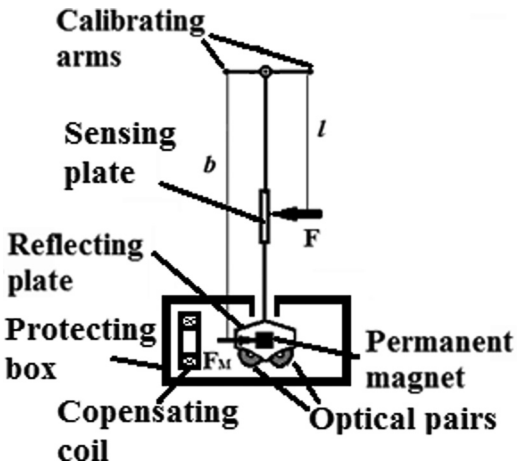

FIG. 2. The Balance Force Meter.

resulting in the two beam lights, each emitted by a Light Emitting Diode (LED) and collected by a photoresistor, to differ in intensity. A LED and a photoresistor are denoted as optical pair in Fig. 2. The displacement of the reflecting plate, and consequently also that of the sensing plate was prevented by driving current through a compensating coil that generated a magnetic force on a permanent magnet that was glued to the reflecting plate. The intensities of the two beam lights being identical indicated that the pendulum was at its equilibrium location and that the two torques were equal-in-size relative to the axis of rotation. We then write

$$F = \frac{b}{l} F_M. \tag{6}$$

Here, F is the force exerted by the flow on the sensing plate and F_M is the opposing force exerted by the current in the compensating coil on the reflecting plate through the glued permanent magnet. As is shown in Fig. 2, the moment arms are l and b ($b = 140$ mm and $l = 82.2$ mm in our BFM).

The force F_M was calibrated, as described in Fig. 3, by employing accurately-measured weights (accuracy of 10^{-4} g). Two equal arms were connected to the upper part of the BFM at the axis of rotation, symmetrically on the opposite sides relative to the axis of rotation, as shown in Fig. 2. One of the arms of the BFM, located at a distance a_f from the axis of rotation ($a_f = 21.7$ mm in our BFM), was loaded with weights, as shown in Fig. 3(a). The compensating coil current I_C was adjusted so that the displacement vanished. From torque equilibrium of the gravity force of the loaded weight and of the magnetic force, F_M, we find

$$F_M = \frac{a_f}{b} m_f g. \tag{7}$$

Here, m_f is the loaded mass and $g = 9.81$ m/s^2. A characteristic for our BFM was measured and is presented in Fig. 3(b). From the characteristic, it was found that in the measured diapason of loaded weights, the magnetic force is a linear function of the coil current $F_M = k_f I_C$ ($k_f = 0.0013$ mN/mA for our BFM). The error in the slope was about 2.5%. If we take into account additional error sources (the inaccuracy

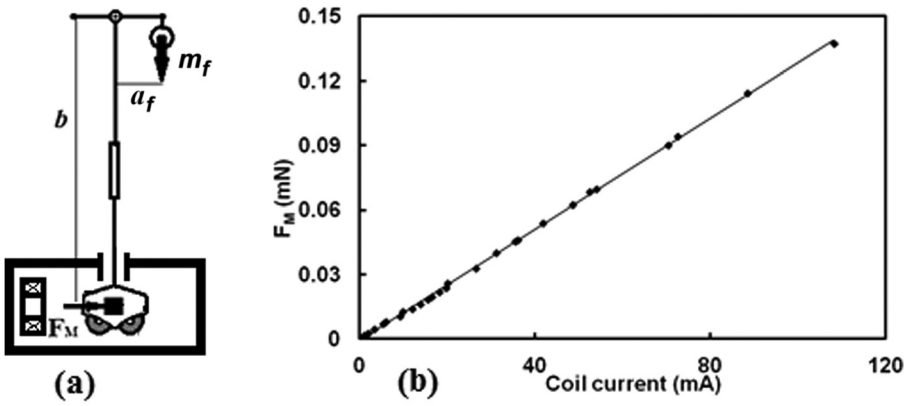

FIG. 3. The BFM calibration: (a) a schematic; (b) the calibration characteristic.

of b, l, and I_C measurements), the error in the measured force F was estimated as 3.5%. Additional considerations indicate that also the error is at least $\pm 1\,\mu$N. A lack of perfect reproducibility in the RPS operation results in an increased error, and we conclude that the force measurements with the RPS have 5% inaccuracy.

A force is exerted on the BFM by the neutral gas that flows out of the RPS even when there is no discharge.[9] The net force exerted by the electric field, F_E [expected to be described by Eq. (1)], was found as the difference between two forces

$$F_E = F_1 - F_2, \tag{8}$$

where F_1 is the force measured when the RPS discharge is on and F_2 is the force measured immediately after the discharge is turned off. Both forces were measured at a distance of 70 mm from the RPS axis. From the inaccuracies of F_1 as 5% and of F_2 as 3.5%, we determine the inaccuracy of F_E as 6% of measured value and not better than $\pm 3\,\mu$N.

C. The ion particle flux and the accelerating voltage

The ion particle flux that flowed out of the RPS into the sensing plate of the BFM, Γ_i, was deduced from $\Gamma_i = I_i/e$, where I_i is the ion current into the upstream side of the BFM. The ion current I_i was found by measuring I_{is}, the current into the upstream side of a Langmuir probe that is placed at the location of the BFM, normal to the radial flow out of the RPS. The current into the upstream side of the Langmuir probe, I_{is}, is deduced from the total current and from the current into the downstream side of the Langmuir probe.[8] The ion current is

$$I_i = \frac{A_F}{A_p} I_{is}, \tag{9}$$

where A_F and A_p are the surface areas of the sensing plate of the BFM and of the Langmuir probe, $A_F/A_p = 1.2$ in our experiment.

The accelerating voltage is

$$V_{ac} = V_A - V_p, \tag{10}$$

where V_A is the potential at the anode and V_p is the plasma potential at the BFM location. The plasma potential was measured by our Langmuir probe that was positioned 70 mm away from the RPS axis, exactly where the sensing plate of the BFM was positioned for the force measurements. Since the cathode was grounded, the potential at the anode V_A equals the discharge voltage. The estimated relative errors were 15% in Γ_i, 10% in V_{ac}, and therefore18% in P_i. With this error in P_i and the previous error estimate of 6% for the force, the deduced F_E/P_i has error of 20%.

We used the Langmuir theory to extract the ion currents I_{is}, and the plasma potential V_p from the probe measurements.[22–24] The details of the analysis are given in the Appendix.

IV. MEASUREMENTS: ELECTRIC FORCE, ION CURRENT, AND ACCELERATING VOLTAGE

In this section, we present measurements of the electric force, the current, and the accelerating voltage, as described in the previous sections. Figures 4 and 5 present our measurements for the argon discharge. In Fig. 4, shown are the electric force on the ion flow that equals the force exerted on the BFM [deduced according to Eq. (8)] and the accelerating voltage [according to Eq. (10)]. Figure 5 shows I_i, the ion current into the upstream side of the BFM [deduced from Eq. (9)], and the pressure in the vacuum chamber measured as described above. In both figures, the results are shown

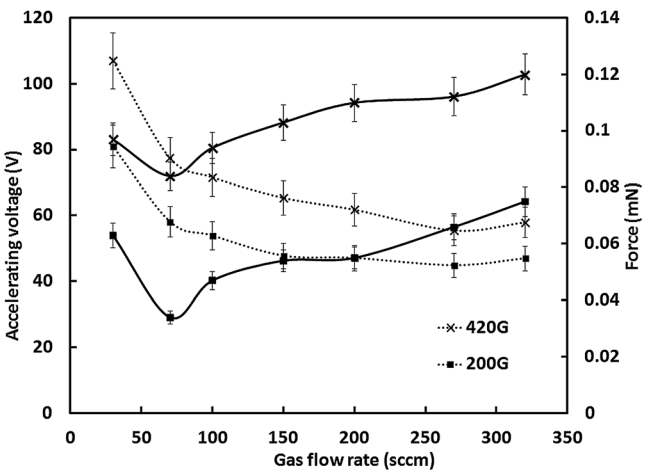

FIG. 4. For argon gas, the accelerating voltage $V_{ac} = V_A - V_p$ (dotted lines) and the force exerted by the flow F_E (solid lines) versus the gas flow rate for various magnetic field intensities.

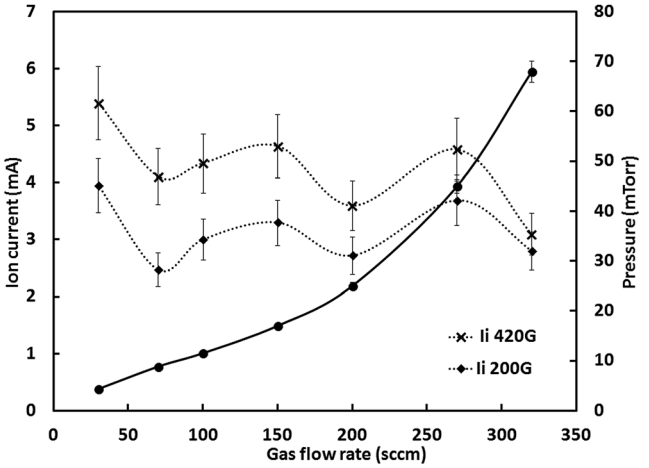

FIG. 5. For argon gas, the ion current I_i (dotted lines) and the pressure in the vacuum chamber P_n (solid line) versus gas flow rate for various magnetic field intensities.

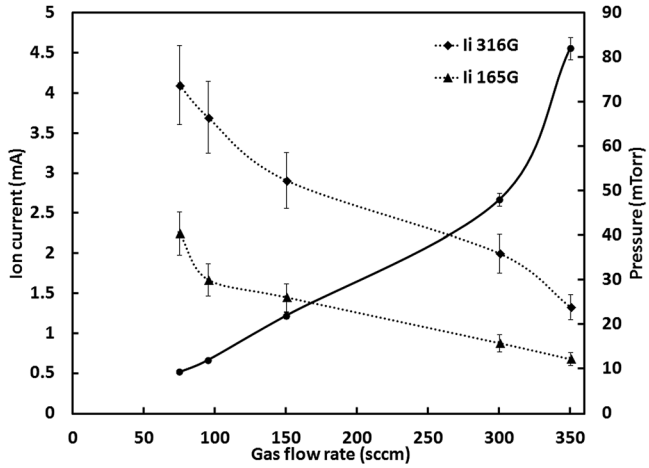

FIG. 7. For nitrogen gas, the ion current I_i (dotted lines) and the pressure in the vacuum chamber P_n (solid line) versus gas flow rate for various magnetic field intensities.

versus the gas flow rate for two magnetic field intensities. The magnetic field intensity denoted is the maximum intensity in the middle plane of the RPS.

Figures 6–9 show equivalent measurements for a nitrogen discharge and a helium discharge, respectively. The results are shown for a small number of magnetic field intensities. Additional measurements that correspond to other values of the magnetic field are shown in Figs. 10–12. The magnetic field intensities are somewhat different for the three different gases, because the discharge is not stable for the same range of magnetic field intensities for all three gases. As mentioned above, the discharge current in all the measurements was 1.1 A.

The dependencies shown in Figs. 4–9 should be explained within a general model of the discharge. Even without such a detailed model, it is apparent from the figures that the ion current, the accelerating voltage and the force all increase with the increase of the magnetic field. In addition, the accelerating voltage decreases with the increase of the gas flow rate. We note that a much higher mass flow rate, and correspondingly a much higher pressure, is needed to maintain the helium discharge. This is because the helium ionization energy is considerably larger than the argon or nitrogen ionization energy.

We now examine whether the results presented in Figs. 4–9 support the relations described in Sec. II and show that indeed the electric force exerted on the flow increases due to ion-neutral collisions.

V. RESULTS AND DISCUSSION

In this section, we demonstrate the enhancement of the momentum delivered to the flow by electric force as a result of ion-neutral collisions. The enhancement is shown to satisfy the relation in Eq. (1). For the values of the quantities in Eq. (5), we substitute the measured force F_E and power into the ions $P_i(=I_iV_{ac})$. The neutral-gas density is not measured inside the RPS and we approximate it as $N = P_n/kT_n$, where P_n is the gas pressure measured in the vacuum chamber, as described in Sec. II, T_n is the (not measured) neutral-gas temperature, and k is the Boltzmann constant. Equation (5) takes therefore the form

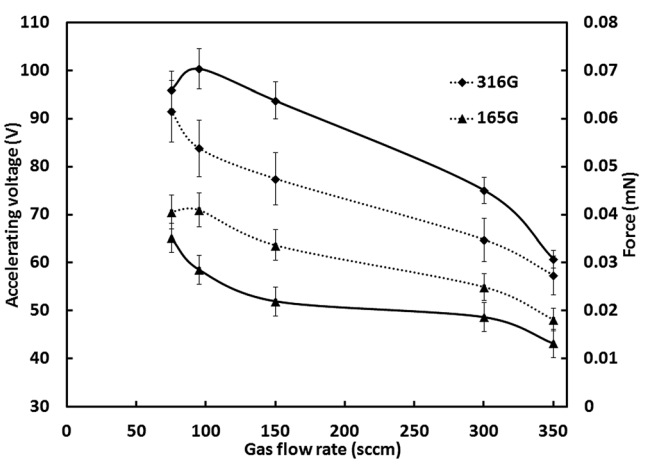

FIG. 6. For nitrogen gas, the accelerating voltage $V_{ac} = V_A - V_p$ (dotted lines) and the force exerted by the flow F_E (solid lines) versus the gas flow rate for various magnetic field intensities.

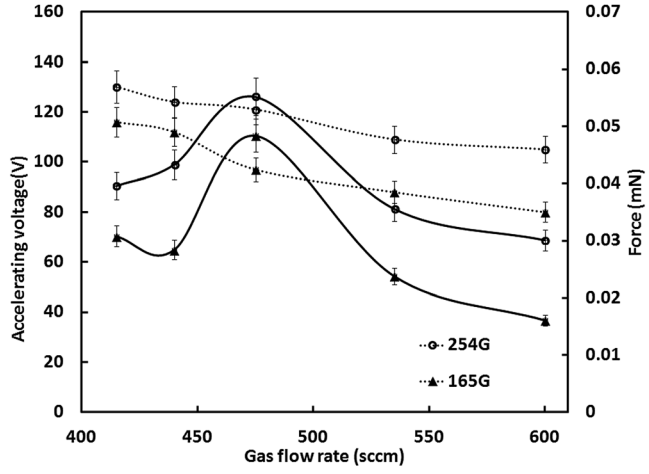

FIG. 8. For helium gas, the accelerating voltage $V_{ac} = V_A - V_p$ (dotted lines) and the force exerted by the flow F_E (solid lines) versus the gas flow rate for various magnetic field intensities.

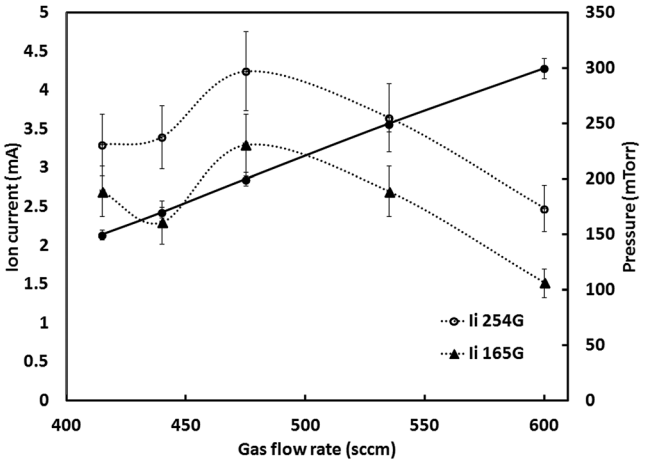

FIG. 9. For helium gas, the ion current I_i (dotted lines) and the pressure in the vacuum chamber P_n (solid line) versus gas flow rate for various magnetic field intensities.

$$\frac{F_E}{P_i} = \sqrt{\frac{m\sigma P_n a}{V_{ac} k T_n}}. \tag{11}$$

Figure 10 shows F_E/P_i as a function of $\sqrt{P_n/V_{ac}}$ for the three different gases. For each one of the three gases, the dependence is indeed approximately linear, confirming our main assertion that the collisions increase the ratio of force over power. The slopes are different for the three gases since the mass m as well as the collision cross section σ are different for the three gases. We note that the dependence is approximately linear even though it is not clear that T_n and a do not vary between the various measurements. The Pearson correlation coefficients are $r = 0.90$ for argon, $r = 0.90$ for nitrogen as well, and $r = 0.69$ for helium. Since Eq. (11) is obtained for several simplifying assumptions, these correlations are high. However, as expected, the correlation coefficient for all the measurements of the three gases is low, $r = -0.12$.

Next, we plot $F_E/P_i\sqrt{u}$ as a function of $\sqrt{P_n/V_{ac}}$ for the three gases (Fig. 11). Here, u is the ion mass number, the ion mass divided by the proton mass (40 for argon, 28 for nitrogen, and 4 for helium). For each one of the three gases,

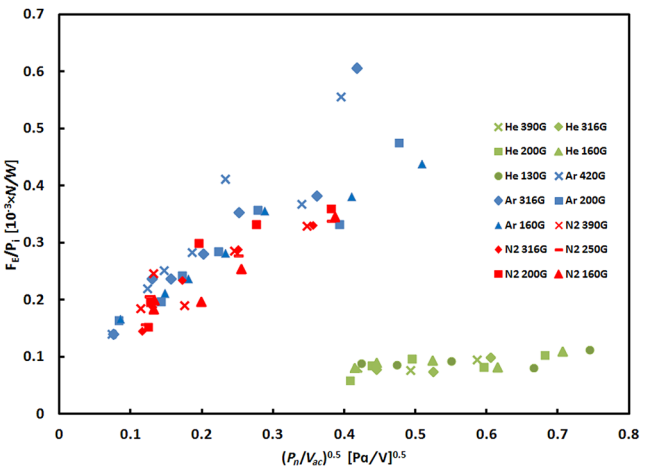

FIG. 10. The force over power.

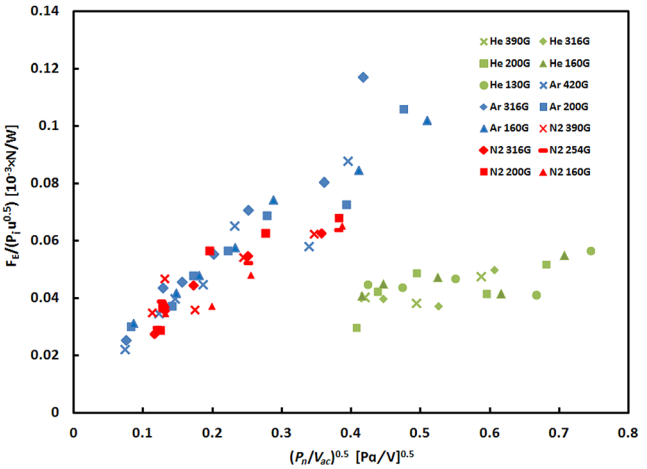

FIG. 11. The force over the power normalized to the square root of the ion mass number.

the dependence is again approximately linear, as before, since all the values for the same gas were simply multiplied by the same factor, $1/\sqrt{u}$. The difference between the slopes of the three gases is smaller than in Fig. 10. Indeed, the Pearson correlation coefficient for all three gases together is $r = 0.43$, relative to $r = -0.12$ in Fig. 10 (the individual correlation coefficients of each gas is the same as before). The increased correlation reflects the incorporating of the effect of the ion mass according to Eq. (1). There is still the effect of the different collision cross-sections to be taken into account.

Figure 12 shows $F_E/P_i\sqrt{u\sigma}$ as a function of $\sqrt{P_n/V_{ac}}$ for the three gases. The collision cross section depends on the ion energy that determines the relative velocity between ions and neutrals. For the regime of ion energies expected in our experiments, the cross section variation is small. Therefore, for each gas, we take a uniform characteristic value. The cross section σ is approximated as 100×10^{-20} m^2 for argon,[25] 90×10^{-20} m^2 for nitrogen,[25] and 30×10^{-20} m^2 for helium.[26] The Pearson correlation coefficient for the three gases together reaches now the high value of $r = 0.91$. Thus, this high correlation indicates that the

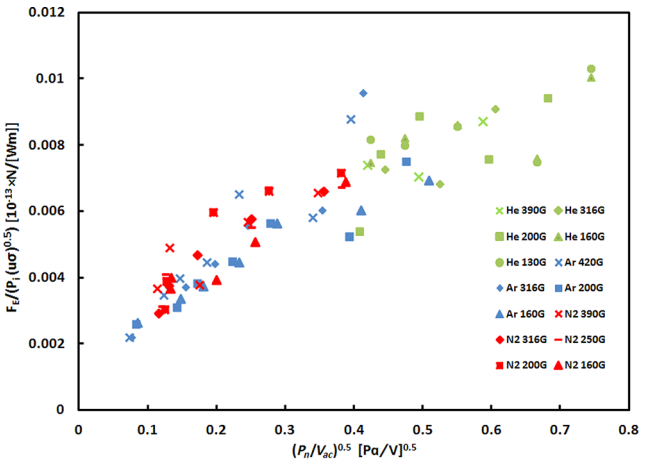

FIG. 12. The force over the power normalized to square root of product of the ion mass number and collision cross-sections.

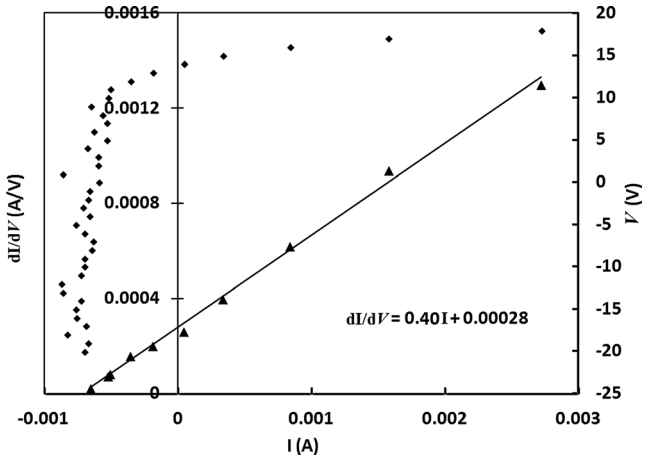

FIG. 13. Example for the analysis of the I-V characteristic of a Langmuir probe and evaluation of I_{is} and T_e for argon gas. Derivative of the probe current with respect to the probe potential versus the probe current (triangles).Written is the expression for the straight line that approximately describes the data. Also shown is the probe potential versus probe current (diamonds). The two equivalent ways yield the same ion current, $I_{is} = 0.7$ mA. Also, at the probe, $T_e \cong 2.5$ eV. The RPS parameters here are a discharge current of 0.6 A, an applied voltage of 60 V, a magnetic field intensity of 115 G and a gas flow rate of 100 sccm.

momentum is enhanced and that this enhancement is described well by our model.

In conclusion, we have demonstrated experimentally the enhancement of momentum delivery to ions due to collisions of ions with neutrals. For the implementation of this enhancement for electric propulsion, the efficiency of the process has to be high. This issue is under investigation.

ACKNOWLEDGMENTS

The authors thank Professor Raymond L. Boxman and Professor Isak Beilis for helpful discussions, and Alexey Oleynik, Constantin Papirov, and Daniel Nissinboim for participation in the measurements. This research has been supported by the Israel Science Foundation (Grant No. 765/11).

APPENDIX: ION CURRENT AND PLASMA POTENTIAL DEDUCED FROM LANGMUIR PROBE MEASUREMENTS

According to Langmuir's theory, the current from the probe to the plasma I, the I-V characteristic, is

$$I = I_{es}\exp\left[-\frac{e(V_p - V)}{kT_e}\right] - I_{is} \quad V < V_p. \tag{A1}$$

Here, I_{is} is the constant-value ion current when the probe potential V is smaller than the plasma potential V_p, and I_{es} is the constant-value electron current when V is larger than V_p. Also, T_e, the electron temperature, is assumed much higher than the ion temperature. When currents into the upstream side of the Langmuir probe are measured, I_{is} is used in Eq. (9) to deduce I_i.

The ion current I_{is} can be found in the standard way as the ion saturation current for negative enough probe voltage, as shown in the example in Fig. 13. We note that I_{is} can also be found by analyzing the I-V characteristic in the neighborhood of the floating potential ($I = 0$). Taking the derivative of I with respect to V in Eq. (A1), we obtain

$$\frac{dI}{dV} = \frac{eI}{kT_e} + \frac{eI_{is}}{kT_e} \quad V < V_p\ . \tag{A2}$$

At the neighborhood of the floating potential, dI/dV is linear with respect to I. We can find I_{is} by extrapolating the straight line to the point where $dI/dV = 0$, so that $I_{is} = -I(dI/dV = 0)$. As both ways are equivalent, we see in Fig. 13 that indeed, I_{is}, deduced by the two ways, is the same. Extracting the value of I_{is} from Eq. (A2) is sometimes advantageous, however, since it is expected to provide the value of I_{is} even if the sheath width becomes too large for a large negative probe voltage,[27] or when one does not want to extract large probe currents, but rather to perform the measurements near the floating potential.

We turn now to the estimate of the plasma potential. We need to know the plasma potential in order to evaluate the accelerating voltage [Eq. (10)]. We easily measure the floating potential V_f and, as a first approximation, we can estimate the accelerating voltage as $V_{ac} = V_A - V_f$. In a non-flowing (argon) plasma, the plasma potential V_p is about $5.2kT_e/e$ higher than the floating potential V_f.[26,28] In order to find T_e, we use the slope of the straight line described by Eq. (A2), similarly to the standard way. In the example in Fig. 13, the electron temperature T_e at the location of the BFM is $T_e \cong 2.5$ eV. Generally, T_e at the location of the BFM is found to vary in our experiments for the three gases between 2 and 5 eV, so that typically $5.2kT_e/e(V_A - V_f) \leq 0.25$. We would like to evaluate more accurately the accelerating voltage by using the value of V_p in the accelerating voltage instead of V_f. The plasma in our experiment is flowing however. The relation between V_p and V_f (generalized to flowing plasmas) is

$$\begin{aligned} V_p &= V_f + \frac{kT_e}{e}\left[\ln\left(\sqrt{\frac{m}{2\pi m_e}}\right) + \frac{1}{2} - \frac{M^2}{2}\right] \quad M \leq 1, \\ V_p &= V_f + \frac{kT_e}{e}\left[\ln\left(\sqrt{\frac{m}{2\pi m_e}}\right) - \ln M\right] \quad M \geq 1. \end{aligned} \tag{A3}$$

Here, $M \equiv v_i/v_B$ is the Mach number, where $v_B \equiv \sqrt{kT_e/m}$. Equations (A3) are easily derived by taking into account the reduction of the presheath voltage in the subsonic regime and the reduction of the sheath voltage in the supersonic regime. The floating potential in a supersonic plasma is higher than in a non-flowing plasma, and we may underestimate the accelerating voltage by $\Delta V_{ac} = (kT_e/e)[1/2 + \ln M]$. From an estimate of the number of collisions in our experiments, $M \leq 3$. Therefore, the error introduced in the accelerating voltage by assuming $V_p - V_f = 5.2\,kT_e/e$, neglecting the plasma flow, turns out to be $\Delta V_{ac}/V_{ac} \leq 0.07$. This is a small error which is within the 10% error estimated in Sec. III C.

[1]J. W. Cuthbertson, R. W. Motley, and W. L. Langer, Rev. Sci. Instrum. **63**, 5279 (1992).
[2]A. Metel, S. Grigoriev, Y. Melnic, V. Panin, and V. Prudnikov, Jpn. J. Appl. Phys., Part 1 **50**, 08JG04 (2011).

[3]M. Tagawa, K. Yokota, N. Ohmae, K. Matsumoto, and M. Suzuki, Tribol. Lett. **17**, 859 (2004).
[4]R. Intrater, G. Lempert, I. Gouzman, E. Grossman, Y. Cohen, D. M. Rein, R. L. Khalfin, and A. Hoffman, High Perform. Polym. **16**, 249 (2004).
[5]A. I. Morozov, Yu. V. Esipchuk, G. N. Tilinin, A. V. Trofimov, Yu. A. Sharov, and G. Ya. Smirnov, Sov. Phys. Tech. Phys. **17**, 482 (1972).
[6]K. Diamant, in *The 46 AIAA/ASME/SAE/ASEE Joint Propulsion Conference & Exhibit*, Nashville, 2010, AIAA Paper No. 2010-6522.
[7]V. Hruby, B. Pote, T. Brogan, K. Hohman, J. Szabo, and P. Rostler, "Air breathing electrically powered Hall effect thruster," U.S. patent 6,834,492 (2004).
[8]G. Makrinich and A. Fruchtman, Phys. Plasmas **16**, 043507 (2009).
[9]G. Makrinich and A. Fruchtman, Appl. Phys. Lett. **95**, 181504 (2009).
[10]A. Fruchtman, IEEE Trans. Plasma Sci. **39**, 530 (2011).
[11]K. E. Burton, "Atmospheric fueled ion engine," U.S. patent 6,145,298 (2000).
[12]D. B. Go, R. A. Maturana, T. S. Fisher, and S. V. Garimella, Int. J. Heat Mass Transfer **51**, 6047 (2008).
[13]C. Kim and J. Hwang, J. Phys. D: Appl. Phys. **45**, 465204 (2012).
[14]J. W. Gregory, C. L. Enloe, G. I. Font, and T. E. McLaughlin, in *The 45th AIAA Aerospace Sciences Meeting and Exhibit*, Reno, 2007, AIAA Paper No. 2007-185.
[15]R. S. Sigmond, J. Appl. Phys. **53**, 891 (1982).
[16]S. A. Cohen, F. Zonca, J. Timberlake, T. Bennett, J. Cuthbertson, W. Langer, and R. Motley, Rev. Sci. Instrum. **61**, 3586 (1990).
[17]D. Chavers and F. Chang-Díaz, Rev. Sci. Instrum. **73**, 3500 (2002).
[18]B. Longmier, B. Reid, A. Gallimore, F. Chang Díaz, J. Squire, T. Glover, G. Chavers, and E. Bering, J. Propul. Power **25**, 746 (2009).
[19]I. S. Nedzelskiy, C. Silva, H. Fernandes, P. Duarte, and C. A. F. Varandas, Rev. Sci. Instrum. **78**, 123505 (2007).
[20]H. S. Marks, I. I. Beilis, and R. L. Boxman, IEEE Trans. Plasma Sci. **37**, 1332 (2009).
[21]Th. Trottenberg, A. Spethmann, V. Schneider, M. Stahl, M. Giesenhagen, and H. Kersten, Contrib. Plasma Phys. **52**, 584 (2012).
[22]N. Hershkowitz, in *Plasma Diagnostics, Discharge parameters and Chemistry*, edited by O. Auciello and D. Flamm (Academic, Boston, 1989), Vol. 1.
[23]I. H. Hutchinson, *Principles of Plasma Diagnostic*, 2nd ed. (Cambridge University Press, Cambridge 2002), Chap. 3.
[24]F. F. Chen, in *Plasma Diagnostic Techniques*, edited by R. H. Huddlestone and S. L. Leonard (Academic, New York, 1965) Chap. 4.
[25]A. V. Phelps, J. Phys. Chem. Ref. Data **20**, 557 (1991).
[26]M. A. Lieberman and A. J. Lichtenberg, *Principles of Plasma Discharges and Materials Processing*, 2nd ed. (Wiley, New York, 2005).
[27]T. E. Sheridan, J. Phys. D: Appl. Phys. **43**, 105204 (2010).
[28]J. P. Sheehan, Y. Raitses, N. Hershkowitz, I. Kaganovich, and N. J. Fisch, Phys. Plasmas **18**, 073501 (2011).